Green synthesis of graphene oxide-$MnFe_2O_4$ composites and their application in removing heavy metal ions

Fangli Liao ✉, *Guiqiang Diao, Hao Li*

School of Chemistry and Materials Engineering, Huizhou University, Huizhou 516007, People's Republic of China
✉ *E-mail: 1628640576@qq.com*

Published in Micro & Nano Letters; Received on 16th October 2018; Revised on 17th February 2019; Accepted on 25th February 2019

The composites of graphene oxide (GO) decorated by $MnFe_2O_4$ have been synthesised via a green and facile strategy that the pristine GO/$MnSO_4$ suspension prepared by Hummers method was directly utilised to convert into the GO-$MnFe_2O_4$ composites. The as-prepared composites were characterised using X-ray diffraction, scanning electron microscopy, Fourier transform infrared spectroscopy, Raman spectra and X-ray photoelectron spectroscopy. The results indicated that the GO-$MnFe_2O_4$ composites were successfully synthesised. The removal behaviours of Pb^{2+} and Cu^{2+} onto GO-$MnFe_2O_4$ were investigated, which indicated that the composites exhibited great adsorption property in aqueous solution. The adsorption process could be fitted well by the pseudo-second-order model and Langmuir isotherm. The thermodynamic studies indicated that the adsorption process of Pb^{2+} and Cu^{2+} onto GO-$MnFe_2O_4$ composites was spontaneous and endothermic in nature. Furthermore, the maximum adsorption capacities for Pb^{2+} and Cu^{2+} calculated from Langmuir model were about 263.85 and 103.41 mg/g at 318 K, respectively. Based on the results from the reusability experiments, the as-prepared GO-$MnFe_2O_4$ composites could be used as a potential adsorbent for removing Pb^{2+} and Cu^{2+} ions from aqueous solutions.

1. Introduction: Water pollution has been an issue of global concern due to the arbitrary disposal of heavy metals and organic pollution from industries and daily life [1]. It is known that heavy metals will cause serious harm to living organisms due to its toxicity, bio-accumulation and carcinogenicity [2]. For the removal of heavy metals, many techniques and common methods, including ion exchange [3], co-precipitation [4], membrane filtration [5] and adsorption have been developed. Among these techniques, adsorption, which is facile to perform and design, has been considered as one of the most attractive and promising methods. Numerous different adsorbents including activated carbon, zeolite, biochar, metallic oxides, organic material, ion exchange resins and different nanostructured materials [6, 7] have been studied for the removal of heavy metals. Since the adsorbents play a vital role in the adsorption process, the development of novel effective adsorbents is essential for water purification.

Graphene, which is an important member of carbon nanomaterial with a single carbon atomic layer in a honeycomb lattice, possesses many outstanding physical and chemical properties [8]. Graphene oxide (GO), which is a significant branch of graphene-based materials and a highly oxidative form of graphene, can be obtained by chemical exfoliation of graphite [9]. There are a large number of oxygen-containing functional groups, such as carboxyl (-COOH), carbonyl (-C = O), epoxy (C–O–C), hydroxyl (-OH) in the graphitic backbone of GO. Large surface area and plenty of active oxygen-containing functional groups allow GO to effectively bind with heavy metal cations through coordination and electrostatic interaction [10, 11]. Although GO is a promising adsorbent for efficient adsorption of heavy metal cations, the drawbacks of easy aggregation and difficulty of separating from water solution significantly limit the application of GO in wastewater treatment. To solve this problem, a valid technique that magnetic nanoparticles were loaded on the surface of GO has been widely reported [12, 13].

Spinel ferrites (MFe_2O_4, where M = Fe^{2+}, Mn^{2+}, Co^{2+}, Ni^{2+} etc.), which are a typical class of magnetic nanoparticles, have been extensively applied in the various fields due to their magnetic properties, excellent chemical stability and electric superiority [14]. Among ferrites, $MnFe_2O_4$ has received considerable attention for potential application in wastewater treatment because of its outstanding properties such as high saturation magnetisation, prominent durability and excellent catalytic activity [15]. Thus, $MnFe_2O_4$ nanoparticles and their derivative materials have been used as efficient adsorbents for the removal of heavy metal ions [16], dyes [15] and pesticides [17] and other contaminants in recent years. Also, among the derivative composite materials of $MnFe_2O_4$, the GO-$MnFe_2O_4$ composites have been synthesised and used as adsorbents to remove the contaminants from aqueous solution. For example, Peng *et al.* [18] have developed a method for the fabrication of hollow three-dimensional (3D) graphene oxide/$MnFe_2O_4$ (GO/$MnFe_2O_4$) by mediating GO suspension with aniline and $MnFe_2O_4$. In this research, the graphene oxide was firstly prepared, then $MnFe_2O_4$ was incorporated into graphene architectures to obtain 3D graphene oxide/$MnFe_2O_4$. Kumar *et al.* [19] have produced GO-$MnFe_2O_4$ magnetic nanohybrids for efficient removal of lead and arsenic from water. Ghobadi *et al.* [16] have investigated the potential of GO-$MnFe_2O_4$ magnetic nanoparticles to remove rare earth element. Ueda Yamaguchi *et al.* [17] have synthesised magnetic $MnFe_2O_4$-graphene hybrid composite and used it as adsorbent for the removal of glyphosate. However, there are two typical characteristics in this Letter. Firstly, the GO is obtained by improved Hummers methods, and secondly, the extra manganese ions such as $MnCl_2$ and $MnSO_4$ are added as the source of $MnFe_2O_4$. It is well known that the pure GO should separate from GO/$MnSO_4$ suspension through fussy and time-consuming procedures in the Hummers methods. Also in this procedure, large quantities of manganese sources are wasted. Therefore, to make highly efficient use of these manganese sources, the pristine GO/$MnSO_4$ made by improved Hummers methods was directly used as the source to prepare GO/$MnFe_2O_4$ in this study. Then, the removal behaviours of Pb^{2+} and Cu^{2+} by GO/$MnFe_2O_4$ were investigated in detail.

2. Experimental procedures: Natural flake graphite (100 mesh, purity>99.95%) was obtained from Nantong Xianghai Carbon Product Co., Ltd; H_2SO_4, $KMnO_4$, H_3PO_4 and H_2O_2 were purchased from Sinopharm Chemical Reagent Co., Ltd. Metal salts including $FeCl_3{\cdot}6H_2O$, $Pb(NO_3)_2$ and $CuSO_4{\cdot}5H_2O$ were provided by Tianjin Fuchen Chemical Reagent Factory. The chemicals were of analytical grade and used without further

purification. All water used was ultra-pure water, which was purified by a Milli-Q water purification system (Millipore, Milford, MA).

2.1. Preparation of pristine GO/$MnSO_4$ suspension: The GO/$MnSO_4$ suspension was prepared by improved Hummer's method from natural flake graphite. Briefly, 9:1 mixture of H_2SO_4/H_3PO_4 was slowly added into a mixture of graphite and $KMnO_4$. The reaction was then heated to 50°C and stirred continuously for 12 h to introduce the oxygen-containing functional groups in the graphitic backbone. After cooling to room temperature, the mixture was poured onto ice cubes and diluted to 250 ml with ultrapure water. And then 30% H_2O_2 was added dropwise until a brilliant yellow GO/$MnSO_4$ suspension was obtained.

2.2. Preparation of GO/$MnFe_2O_4$ composites: The GO/$MnFe_2O_4$ composites were prepared through a facile hydrothermal method. Firstly, 10 mol/l NaOH was slowly dropped into the 10 ml GO/$MnSO_4$ suspension (the concentration of Mn^{2+} was about 4.05 mg/l) until a final pH = 8–9 was reached and then the suspension was centrifuged to dislodge the supernatant (which contained a great number of Na_2SO_4). Secondly, the acquired brown precipitate was diluted to 18 ml and then 0.4 g $FeCl_3{\cdot}6H_2O$ was added. After that, an appropriate amount of NaOH was added until the pH of mixture maintained at about 11. Finally, the resulting dispersion was transferred to a 25 ml Teflon-lined stainless-steel autoclave and maintained at 180°C for 8 h. After cooling to room temperature, the obtained products were washed with ultra-pure water and centrifuged several times, and then the materials were dried under vacuum-freeze for 48 h.

2.3. Characterisation methods: The surface morphologies of the materials were observed by field emission scanning electron microscopy (SEM, MIRA3 TESCAN). The phase, crystal structure and crystallinity of as-synthesised materials were determined by X-ray diffraction (XRD, Rigaku D/max 2550). Fourier transform infrared (FT-IR) spectra were collected between 400 and 4000 cm^{-1} on a Nicolet 6700 FT-IR spectroscopy. Raman spectroscopy was obtained on a LabRam HR 800 spectrometer. X-ray photoelectron spectrometry (XPS) was carried out on an XPS system (Pekin-Elmer ESCA 5000c).

2.4. Adsorption studies: To assess the adsorption capacity of as-prepared materials, the batch adsorption experiments were carried out individually in 100 ml conical flask, each containing 5 mg adsorbent and 25 ml of Pb^{2+} or Cu^{2+} solution with various concentrations. The mixture was shaken for a certain time in a thermostat shaker. After equilibrium, the final supernatant was filtered through a 0.45 μm filter membrane and the concentration of heavy metal ions was determined by ICP-AES. The adsorption capacity of adsorbent was calculated using the following equation:

$$q_e = \frac{C_0 - C_e}{m} \times V \quad (1)$$

where C_0 (mg/l) and C_e (mg/l) are original and equilibrium concentrations of heavy metal ions, respectively, V (L) is the volume of the solution, m (g) is the mass of the adsorbent, q_e (mg/g) is the amount of heavy metal ions adsorbed per unit amount of adsorbent. All the experimental data were the average of triplicate determinations.

3. Results and discussion: The XRD patterns of pure GO, bare $MnFe_2O_4$ and GO-$MnFe_2O_4$ are shown in Fig. 1. In the pattern of pure GO, the peak at 2Θ = 9.82° indexed to the (002) pattern of GO was found, confirming the existence of oxygen-containing groups of graphene oxide [20]. In the XRD pattern of bare $MnFe_2O_4$, the diffraction peaks at 2Θ = 18.04°, 29.75°, 35.02°, 42.58°, 52.74°, 56.27°, 61.76° and 73.06° could correspond

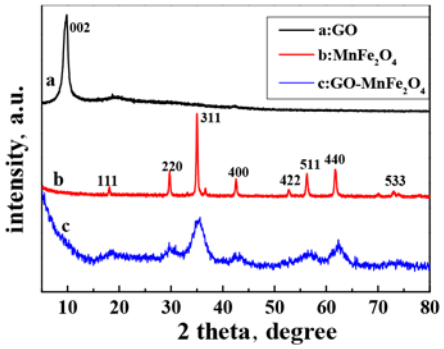

Fig. 1 *XRD patterns of*
a GO
b $MnFe_2O_4$
c GO-$MnFe_2O_4$

to (111), (220), (311), (400), (422), (511), (440) and (533) crystal planes of $MnFe_2O_4$, respectively [16, 17]. In the XRD pattern of GO-$MnFe_2O_4$, all diffraction peaks of $MnFe_2O_4$ and no other peaks of impurities were observed, which indicated the pure cubic spinel crystal structure of $MnFe_2O_4$ was formed in the GO-$MnFe_2O_4$ composites [21, 22]. Also compared with pure $MnFe_2O_4$, the relatively weaker intensity of diffraction peaks of $MnFe_2O_4$ was observed in GO-$MnFe_2O_4$ composites, suggesting a lower crystallinity of the hybrid materials [23]. Noticeably, the characteristic peaks of GO disappeared in the composites. This phenomenon could be attributed to the hydrothermal reduction of GO or the strong signals of the manganese ferrite overwhelming the weak GO peaks [12].

The surface morphologies of as-prepared GO-$MnFe_2O_4$ composites were characterised by SEM images. As shown in Fig. 2, GO exhibited transparent ultrathin nanosheet with a smooth surface and many wrinkles, which indicated the graphite was successfully exfoliated into graphene oxide [24]. For GO-$MnFe_2O_4$, it was observed that the structure of GO sheets remained, but the composites had rougher and more wrinkled surface compared to the pure GO and many irregularity $MnFe_2O_4$ particles were fully anchored on the surface of GO nanosheet. Furthermore, the GO-$MnFe_2O_4$ composites exhibited a loose stacking of sheets and porous structure, which might be beneficial to improve adsorption capacities of materials.

The FT-IR spectra of the samples are shown in Fig. 3. In the spectrum of GO, the characteristic absorption peaks at 3402 cm^{-1}, 1734 cm^{-1}, 1620 cm^{-1}, 1400 cm^{-1} and 1114 cm^{-1} were attributed to the hydroxyl group (O-H), the stretching vibration of carbonyl (C = O) groups, aromatic C = C, C–O–C asymmetric stretching and alkoxy group (C–O), respectively [25]. The results clearly revealed that the oxygen-containing functional groups were successfully grafted on the GO sheet [26]. Compared with the FT-IR spectrum of GO, the bands related to

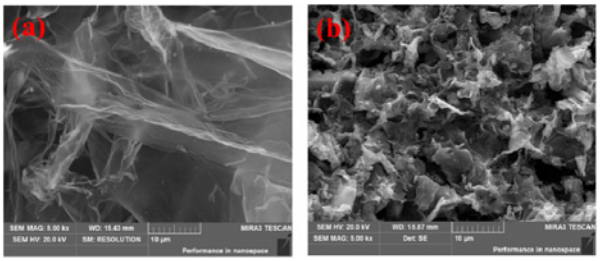

Fig. 2 *SEM images of*
a GO
b GO-$MnFe_2O_4$

doi: 10.1049/mnl.2018.5640

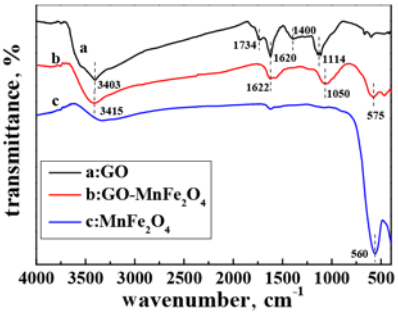

Fig. 3 *FT-IR spectra of*
a GO
b GO-$MnFe_2O_4$
c $MnFe_2O_4$

oxygen-containing functional groups (-COOH and C–O–C) were obviously disappeared in the FT-IR spectrum of GO-$MnFe_2O_4$, revealing that thermal reduction of GO occurred in the hydrothermal process [17]. Also the new characteristic peak at 575 cm^{-1} observed in GO-$MnFe_2O_4$ composite was assigned to the metal–oxygen stretching vibrations of manganese ferrite, which indicated the GO-$MnFe_2O_4$ composite was successfully synthesised [22].

The Raman spectroscopy was used to investigate the structure and vibrational properties of as-prepared materials. It is well known that the D band is associated with the vibration of sp^3 carbon atoms of defects and order/disorder of the system, while the G band is related to the vibration of sp^2 carbon atoms in a graphitic 2D hexagonal lattice [27, 28]. In addition, the intensity ratio of D band and G band (I_D/I_G) is used to evaluate the relative degree of structural defects and the quality of carbon materials [29]. As shown in Fig. 4, the intensity ratio increased from 0.86 (GO) to 1.17 (GO-$MnFe_2O_4$), representing an increase of defect on the surface of GO after the introduction of $MnFe_2O_4$ particles. Furthermore, a new peak appearing at 624 cm^{-1} in the spectrum of GO-$MnFe_2O_4$ could be ascribed to the characteristic peak of $MnFe_2O_4$, which implied that the presence of $MnFe_2O_4$ in the composites [16, 30].

The detailed elemental composition and surface electronic state of GO-$MnFe_2O_4$ composites were investigated by XPS. Also the corresponding XPS results were performed as shown in Fig. 5. In the survey spectrum of GO, there were only two elements, named C and O. Compared with GO, the survey spectrum of GO-$MnFe_2O_4$ not only exhibited the C and O signals but also exhibited two additional peaks with binding energies of 642 and 711 eV, corresponding to Mn 2p and Fe 2p signals, respectively, indicating the presence of $MnFe_2O_4$ in the composites [31].

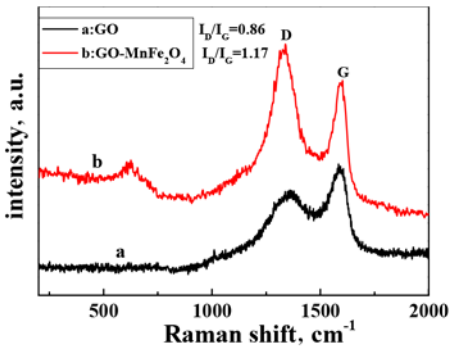

Fig. 4 *Raman spectra of*
a GO
b GO-$MnFe_2O_4$

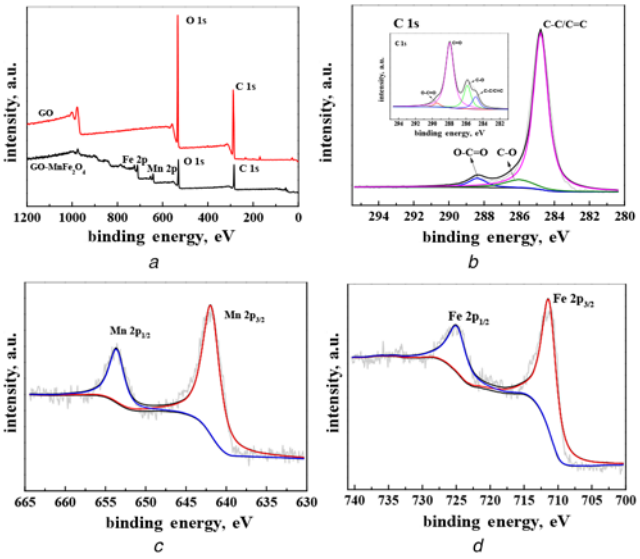

Fig. 5 *XPS spectra of RGO/$MnFe_2O_4$, GO*
a Survey scan
b–d C 1s region, Mn 2p region, Fe 2p region of GO/$MnFe_2O_4$; the inset in (*b*) is C 1s region of GO

Furthermore, in the C 1s deconvoluted spectrum of GO-$MnFe_2O_4$, the intensity of peaks of C 1s of the O–C = O and C–O forms decreased significantly, while the peak associated with C–C/C = C became predominant, indicating an occurrence of thermal reduction of GO during the hydrothermal process [32]. In the spectrum of Mn 2p (Fig. 4*c*), the doublet peaks appeared at 641.9 eV for Mn $2p_{3/2}$ and 653.6 eV for Mn $2p_{1/2}$, conforming the oxidation state of Mn^{2+} in $MnFe_2O_4$ [33]. Moreover, for Fe 2p spectra, two peaks with binding energies of 711.3 and 724.9 eV appeared, corresponding to Fe $2p_{3/2}$ and Fe $2p_{1/2}$ of Fe^{3+}, respectively. The obtained results again clearly provided evidence of the existence of $MnFe_2O_4$ in the composites [34, 35].

3.1. Adsorption kinetics: To study the mechanism of adsorption kinetic, two widely accepted kinetic model including pseudo-first-order and pseudo-second-order models were used to test experimental data. The pseudo-first-order kinetic model could be generally expressed as follows:

$$\log(q_e - q_t) = \log(q_e) - \frac{k_1 t}{2.303} \tag{2}$$

The pseudo-second-order kinetic model was given as the following equation:

$$\frac{t}{q_t} = \frac{1}{k_2 q_e^2} + \frac{t}{q_e} \tag{3}$$

where q_e (mg/g) and q_t (mg/g) refer to the adsorbed amount of heavy metal ions on the adsorbent at equilibrium time and at time t (min), respectively. k_1 (1/min) and k_2 (g/mg/min) are the rate constant of pseudo-first-order and pseudo-second-order kinetic models, respectively.

The adsorption data of Pb^{2+} and Cu^{2+} at different time are shown in Fig. 6*a*. It was seen from Fig. 6*a* that the necessary time to reach equilibrium was about 8 h. Therefore, 10 h was chosen for the following experiment to ensure sorption equilibrium. The calculated parameters of the above kinetic model are tabulated in Table 1, and the fitting lines are shown in Figs. 6*b* and *c*. It was observed that the adsorption data of Pb^{2+} and Cu^{2+} on the GO-$MnFe_2O_4$ composites could be fitted better by the pseudo-second-order

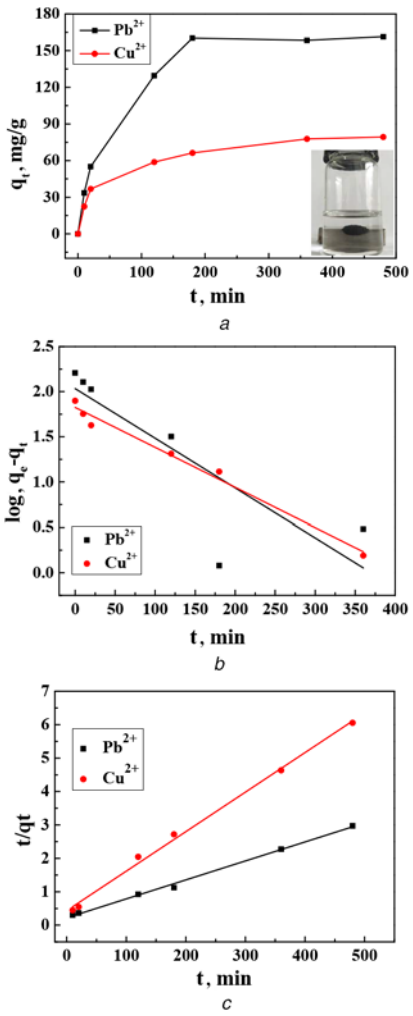

Fig. 6 *Adsorption of Pb^{2+} and Cu^{2+} ions onto GO-$MnFe_2O_4$*
a Effect of time on the adsorption of Pb^{2+} and Cu^{2+} by GO-$MnFe_2O_4$ composite and the inset reveals the magnetic separation of GO-$MnFe_2O_4$ composites (initial concentration: 0.3 mmol/l; adsorbent: 5 mg/ 25 ml; temperature: 25°C)
b pseudo-first-order kinetic model
c pseudo-second-order kinetic model

Table 1 Kinetic parameters for the adsorption of Pb^{2+} and Cu^{2+} onto GO-$MnFe_2O_4$ composites ($[Pb^{2+}]=[Cu^{2+}]=0.3$ mmol l^{-1})

Equations	Parameters	Pb(II)	Cu(II)
first-order-kinetic	q_e (mg/g)	108.07	66.91
	k_1 (min^{-1})	0.0127	0.0102
	R^2	0.6407	0.9824
second-order-kinetic	q_e (mg/g)	176.05	84.53
	k_2 (min^{-1})	1.57×10^{-4}	3.22×10^{-4}
	R^2	0.9964	0.9953

kinetic model with higher correlation coefficient ($R^2>0.99$) than that of pseudo-first-order kinetic model, suggesting that the adsorption process of Pb^{2+} and Cu^{2+} onto GO-$MnFe_2O_4$ composites were mainly controlled by chemisorption [13, 36].

3.2. Adsorption isotherm: Equilibrium adsorption isotherms are used to determine the capacities of adsorbents and provide the important parameters for the determination of basic adsorption mechanism. In this work, two equilibrium adsorption models, including Langmuir isotherms (4) and Freundlich isotherms (5)

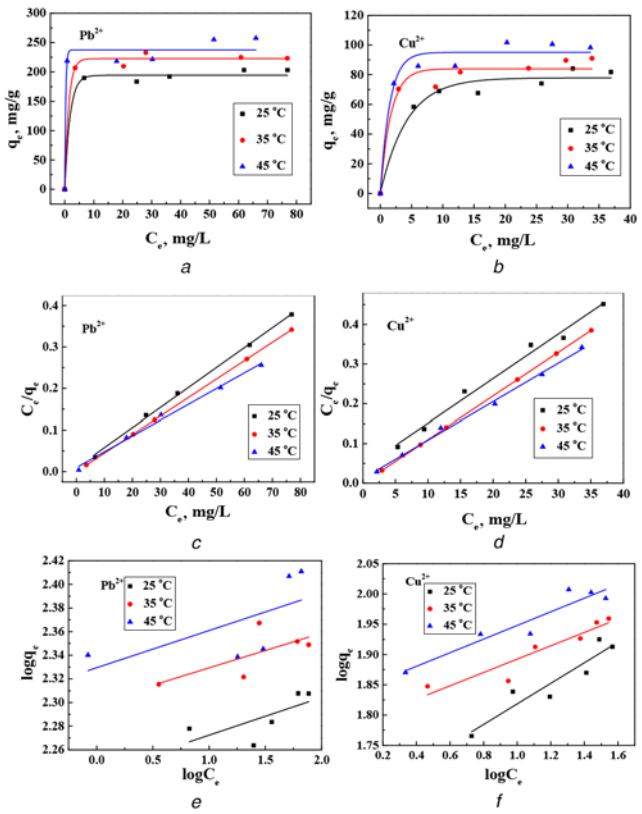

Fig. 7 *Adsorption isotherms of*
a Pb^{2+}
b Cu^{2+} onto GO-$MnFe_2O_4$ composites at three different temperatures (initial concentration: 0.20–1.00 mmol/l; adsorbent: 5 mg/25 ml; adsorption equilibrium:10 h); fitting of isotherms data of
c Pb^{2+}
d $Cu^{2+}$with linear Langmuir model; fitting of isotherms data of
e Pb^{2+}
f Cu^{2+} with linear Freundlich model

were chosen to describe the adsorption equilibrium data for Pb^{2+} and Cu^{2+} adsorption onto GO-$MnFe_2O_4$ composites.

$$\frac{C_e}{q_e}=\frac{C_e}{q_m}+\frac{1}{k_L q_m} \tag{4}$$

$$\log q_e=\frac{1}{n}\log C_e+\log k_f \tag{5}$$

where C_e (mg/l) is the equilibrium concentration of heavy metal ions and q_e (mg/g) is the corresponding adsorption capacity; q_m (mg/g) is the theoretical maximum Langmuir monolayer adsorption capacity, k_L is the Langmuir constant related with adsorption strength, k_f (mg/g·(mg/l)^n) and n are the constants of Freundlich isotherm indicating adsorption capacity and effectiveness, respectively.

The fitting plots are shown in Fig. 7 and the parameters are summarised in Table 2. It was observed that the adsorption equilibrium data for Pb^{2+} and Cu^{2+} adsorption onto GO-$MnFe_2O_4$ composites could be fitted satisfactorily by Langmuir isotherms with higher regression correlations ($R^2>0.98$) compared to Freundlich isotherms ($R^2<0.88$), indicating that the adsorption of Pb^{2+} and Cu^{2+} was monolayer adsorption. In other words, the adsorption took place on specific homogeneous sites within the GO-$MnFe_2O_4$ composites [37, 38].

3.3. Adsorption thermodynamic parameters: The thermodynamic parameters (ΔH^θ, ΔS^θ, ΔG^θ) for adsorption could be calculated

doi: 10.1049/mnl.2018.5640

Table 2 Isotherm results and parameters of the adsorption of Pb^{2+} and Cu^{2+} onto GO-$MnFe_2O_4$ composites

	T, °C	Langmuir model			Freundlich model		
		q_m(mg/g)	k_L	R^2	k_f	n	R^2
Pb^{2+}	25	207.47	0.5015	0.9980	173.94	31.30	0.3091
—	35	224.72	-4×10^{13}	0.9999	199.49	34.01	0.3406
—	45	263.85	0.3887	0.9907	213.52	31.76	0.2325
Cu^{2+}	25	89.13	0.2870	0.9858	44.53	5.89	0.8557
—	35	91.07	0	0.9999	60.55	9.07	0.8516
—	45	103.41	0.8153	0.9953	68.45	8.88	0.8715

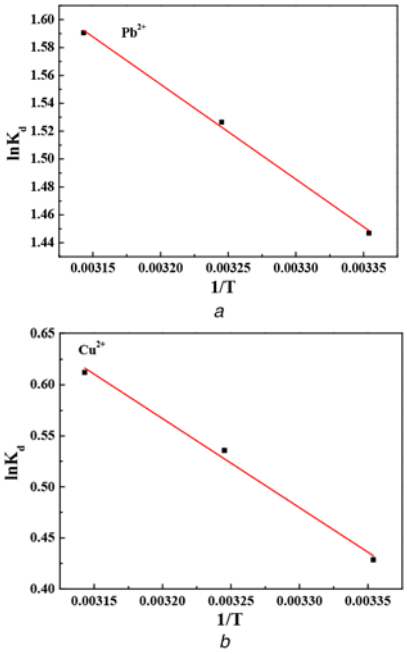

Fig. 8 *Plots of lnk$_d$ versus 1/T*
a Of Pb^{2+}
b Of Cu^{2+}

from the temperature-dependent adsorption isotherms. They are used to define whether the adsorption process is exothermic or endothermic and spontaneous. The values of thermodynamic parameters and equilibrium distribution coefficient k_d could be calculated by the following equation:

$$k_d = \frac{C_0 - C_e}{C_e} \times \frac{V}{m} \tag{6}$$

$$\ln k_d = \frac{\Delta S^\theta}{R} - \frac{\Delta H^\theta}{RT} \tag{7}$$

$$\Delta G^\theta = \Delta H^\theta - T\Delta S^\theta \tag{8}$$

where C_0, C_e, V and m are consistent with (1), T is the absolute temperature (K) and R is the universal gas constant (8.314 J/mol K). The values of ΔH^θ and ΔS^θ could be obtained from the intercept and slope of the linear plot of ln k_d versus $1/T$ in Fig. 8. And the calculated results of ΔH^θ, ΔS^θ *and* ΔG^θ are shown in Table 3. The positive values of ΔH^θ confirmed the endothermic nature of adsorption process and the positive values of ΔS^θ indicated that the degrees of freedom of the solid-solution system increased during the adsorption of Pb^{2+} and Cu^{2+} ions onto GO-$MnFe_2O_4$ [39, 40]. Furthermore, the adsorption process was found spontaneous and thermodynamically favourable in nature with negative values of ΔG^θ and the lower values of ΔG^θ were obtained at higher temperature suggested that more energetically favourable adsorption at a higher temperature.

Table 3 Obtained thermodynamic parameters of Pb^{2+} and Cu^{2+} adsorption onto GO-$MnFe_2O_4$ composites

Metal ions	T (K)	ΔG^θ (kJ/mol)	ΔH^θ (kJ/mol)	ΔS^θ (J/K·mol)	R^2
Pb^{2+}	298	−3.586	—	—	—
—	308	−3.897	5.664	31.040	0.9962
—	318	−4.207	—	—	—
Cu^{2+}	298	−1.068	—	—	—
—	308	−1.347	7.256	27.932	0.9882
—	318	−1.626	—	—	—

3.4. Reusability of GO-$MnFe_2O_4$ composites: To evaluate the practical reusability of GO-$MnFe_2O_4$ composites, the consecutive adsorption–desorption experiments were operated. After adsorption, the metal ions loaded GO-$MnFe_2O_4$ composites were filtered and then immersed into 0.2 mol/l HCl solution for 2 h. Then, the adsorbent was filtered, washed several times with ultra-pure water and vacuum-freeze dried for 24 h. Finally, the obtained adsorbent was reused at 318 K. It was found that the adsorption capacities of GO-$MnFe_2O_4$ composites were still above 200 and 80 mg/g for Pb^{2+} and Cu^{2+} after five consecutive cycles of adsorption–desorption, respectively. Accordingly, GO-$MnFe_2O_4$ composites could be repeatedly used as an efficient adsorbent to remove metal ions.

3.5. Real capability of the composites in multi-metal ions system: To evaluate the real adsorption capability in multi-metal ions system. 5 mg adsorbent was added into 25 ml solution including Pb^{2+} and Cu^{2+}, and then the mixture was shaken for 10 h at 298 K. The initial concentrations of Pb^{2+} and Cu^{2+} were both 30.0 mg/l. It was found that the adsorption capabilities of the composites for Pb^{2+} and Cu^{2+} were 183.74 and 72.20 mg/g, respectively.

4. Conclusion: The pristine GO/$MnSO_4$ suspension prepared by improved Hummers method was directly used to synthesise the GO/$MnFe_2O_4$ composites. This method not only avoided the fussy and time-consuming procedure that GO separated from GO/$MnSO_4$ suspension but also efficiently utilised the manganese source in GO/$MnSO_4$ suspension. The as-prepared GO-$MnFe_2O_4$ composites exhibited excellent adsorption capacity for Pb^{2+} and Cu^{2+}. The adsorption data could be fitted well with the pseudo-second-order kinetic model and Langmuir isotherm, indicating a chemisorption and monolayer adsorption process. The thermodynamic parameters indicated that the adsorption process was endothermic, spontaneous and thermodynamically

favourable. In addition, in multi-metal ions system, the adsorption capacities of composites for Pb^{2+} and Cu^{2+} were still above 100 and 15 mg/g, respectively. The study demonstrated that GO-$MnFe_2O_4$ composites could be used as a potential adsorbent for removing heavy metal ions in aqueous solution.

5. Acknowledgment: This work was supported by the Educational and Teaching Research and Reform Projects of Guangdong Provincial Education Department (grant no. [2018]180) and the Program for Innovative Research Team of Huizhou University.

6 References

[1] Fu F., Wang Q.: 'Removal of heavy metal ions from wastewaters: a review', *J. Environ. Manage.*, 2011, **92**, (3), pp. 407–418
[2] Bhattacharyya K.G., Gupta S.S.: 'Adsorption of a few heavy metals on natural and modified kaolinite and montmorillonite: a review', *Adv. Colloid Interface Sci.*, 2008, **140**, pp. 114–131
[3] Dabrowski A., Hubicki Z., Podkoscielny P., *ET AL.*: 'Selective removal of the heavy metal ions from waters and industrial wastewaters by ion-exchange method', *Chemosphere*, 2004, **56**, (2), pp. 91–106
[4] Charerntanyarak L.: 'Heavy metals removal by chemical coagulation and precipitation', *Water Sci. Technol.*, 1999, **39**, (10-11), pp. 135–138
[5] Blöcher C., Dorda J., Mavrov V., *ET AL.*: 'Hybrid flotation – membrane filtration process for the removal of heavy metal ions from wastewater', *Water Res.*, 2003, **37**, (16), pp. 4018–4026
[6] Thekkudan V.N., Vaidyanathan V.K., Ponnusamy S.K., *ET AL.*: 'Review on nanoadsorbents: a solution for heavy metal removal from wastewater', *IET Nanobiotechnol.*, 2017, **11**, (3), pp. 213–224
[7] ZLiang C.Y., Feng X.Z., Yu J.G., *ET AL.*: 'Facile one-step hydrothermal syntheses of graphene oxide–MnO_2 composite and their application in removing heavy metal ions', *Micro Nano Lett.*, 2018, **13**, (8), pp. 1179–1184
[8] Loh K.P., Bao Q., Ang P.K., *ET AL.*: 'The chemistry of graphene', *J. Mater. Chem.*, 2010, **20**, (12), pp. 2277–2289
[9] Dreyer D.R., Park S., Bielawski C.W., *ET AL.*: 'The chemistry of graphene oxide', *Chem. Soc. Rev.*, 2010, **39**, (1), pp. 228–240
[10] Chowdhury S., Balasubramanian R.: 'Recent advances in the use of graphene-family nanoadsorbents for removal of toxic pollutants from wastewater', *Adv. Colloid Interface Sci.*, 2014, **204**, pp. 35–56
[11] Zhou F., Yu J., Jiang X.: 'Green synthesis of 3D porous graphene/lignin composites with improved adsorption capacity for heavy metal ions in aqueous solution', *Desalin. Water Treat.*, 2018, **103**, pp. 175–181
[12] Deng J.-H., Zhang X.-R., Zeng G.-M., *ET AL.*: 'Simultaneous removal of Cd(II) and ionic dyes from aqueous solution using magnetic graphene oxide nanocomposite as an adsorbent', *Chem. Eng. J.*, 2013, **226**, pp. 189–200
[13] Zhang Y., Yan L., Xu W., *ET AL.*: 'Adsorption of Pb(II) and Hg(II) from aqueous solution using magnetic $CoFe_2O_4$-reduced graphene oxide', *J. Mol. Liq.*, 2014, **191**, pp. 177–182
[14] Jung K.W., Lee S.Y., Lee Y.J.: 'Facile one-pot hydrothermal synthesis of cubic spinel-type manganese ferrite/biochar composites for environmental remediation of heavy metals from aqueous solutions', *Bioresour. Technol.*, 2018, **261**, pp. 1–9
[15] Lamdab U., Wetchakun K., Kangwansupamonkon W., *ET AL.*: 'Effect of a pH-controlled co-precipitation process on rhodamine B adsorption of $MnFe_2O_4$ nanoparticles', *RSC Adv.*, 2018, **8**, (12), pp. 6709–6718
[16] Ghobadi M., Gharabaghi M., Abdollahi H., *ET AL.*: '$MnFe_2O_4$-graphene oxide magnetic nanoparticles as a high-performance adsorbent for rare earth elements: synthesis, isotherms, kinetics, thermodynamics and desorption', *J. Hazard. Mater.*, 2018, **351**, pp. 308–316
[17] Ueda Yamaguchi N., Bergamasco R., Hamoudi S.: 'Magnetic $MnFe_2O_4$ –graphene hybrid composite for efficient removal of glyphosate from water', *Chem. Eng. J.*, 2016, **295**, pp. 391–402
[18] Peng X., Gao F., Zhao J., *ET AL.*: 'Self-assembly of a graphene oxide/$MnFe_2O_4$ motor by coupling shear force with capillarity for removal of toxic heavy metals', *J. Mater. Chem. A*, 2018, **6**, (42), pp. 20861–20868
[19] Kumar S., Nair R.R., Pillai P.B., *ET AL.*: 'Graphene oxide-$MnFe_2O_4$ magnetic nanohybrids for efficient removal of lead and arsenic from water', *ACS Appl. Mater. Interfaces*, 2014, **6**, (20), pp. 17426–17436
[20] Pourbeyram S.: 'Effective removal of heavy metals from aqueous solutions by graphene oxide–zirconium phosphate (GO–Zr-P) nanocomposite', *Ind. Eng. Chem. Res.*, 2016, **55**, pp. 5608–5617
[21] Santhosh C., Kollu P., Felix S., *ET AL.*: '$CoFe_2O_4$ and $NiFe_2O_4$@graphene adsorbents for heavy metal ions – kinetic and thermodynamic analysis', *RSC Adv.*, 2015, **5**, (37), pp. 28965–28972
[22] Huong P.T.L., Huy L.T., Phan V.N., *ET AL.*: 'Application of graphene oxide-$MnFe_2O_4$ magnetic nanohybrids as magnetically separable adsorbent for highly efficient removal of arsenic from water', *J. Electron. Mater.*, 2016, **45**, (5), pp. 2372–2380
[23] Tan L., Wang Y., Liu Q., *ET AL.*: 'Enhanced adsorption of uranium (VI) using a three-dimensional layered double hydroxide/graphene hybrid material', *Chem. Eng. J.*, 2015, **259**, pp. 752–760
[24] Yang K., Chen B., Zhu X., *ET AL.*: 'Aggregation, adsorption, and morphological transformation of graphene oxide in aqueous solutions containing different metal cations', *Environ. Sci. Technol.*, 2016, **50**, (20), pp. 11066–11075
[25] Zhou F., Feng X., Yu J., *ET AL.*: 'High performance of 3D porous graphene/lignin/sodium alginate composite for adsorption of Cd(II) and Pb(II)', *Environ. Sci. Pollut. Res. Int.*, 2018, **25**, (16), pp. 15651–15661
[26] Huang X., Pan M.: 'The highly efficient adsorption of Pb(II) on graphene oxides: a process combined by batch experiments and modeling techniques', *J. Mol. Liq.*, 2016, **215**, pp. 410–416
[27] Liu J., Ge X., Ye X., *ET AL.*: '3D graphene/δ-MnO_2 aerogels for highly efficient and reversible removal of heavy metal ions', *J. Mater. Chem. A*, 2016, **4**, pp. 1970–1979
[28] Wu S., Zhang K., Wang X., *ET AL.*: 'Enhanced adsorption of cadmium ions by 3D sulfonated reduced graphene oxide', *Chem. Eng. J.*, 2015, **262**, pp. 1292–1302
[29] He H., Huang J., Lu J.: 'Photo- and photo-Fenton-like catalytic degradations of malachite green in a water using magnetically separable $ZnFe_2O_4$-reduced graphene oxide hybrid nanostructuresa', *J. Sci. Res. Rep.*, 2016, **10**, (2), pp. 1–11
[30] Yao Y., Cai Y., Lu F., *ET AL.*: 'Magnetic recoverable $MnFe_2O_4$ and $MnFe_2O_4$-graphene hybrid as heterogeneous catalysts of peroxymonosulfate activation for efficient degradation of aqueous organic pollutants', *J. Hazard. Mater.*, 2014, **270**, pp. 61–70
[31] Wu K., Hu G., Cao Y., *ET AL.*: 'Facile and green synthesis of $MnFe_2O_4$/reduced graphene oxide nanocomposite as anode materials for Li-ion batteries', *Mater. Lett.*, 2015, **161**, pp. 178–180
[32] Peng X., Qu J., Tian S., *ET AL.*: 'Green fabrication of magnetic recoverable graphene/$MnFe_2O_4$ hybrids for efficient decomposition of methylene blue and the Mn/Fe redox synergetic mechanism', *RSC Adv.*, 2016, **6**, (106), pp. 104549–104555
[33] Wan C., Jiao Y., Li J.: 'Synthesis of $MnFe_2O_4$/cellulose aerogel nanocomposite with strong magnetic responsiveness', *Front. Agric. Sci. Eng.*, 2017, **4**, (1), pp. 116–120
[34] Ozcan S., Akansel S., Ceylan A.: 'The influence of reactive milling on the structure and magnetic properties of nanocrystalline $MnFe_2O_4$', *Ceram. Int.*, 2013, **39**, (5), pp. 5335–5341
[35] Ren Y., Li N., Feng J., *ET AL.*: 'Adsorption of Pb(II) and Cu(II) from aqueous solution on magnetic porous ferrospinel $MnFe_2O_4$', *J. Colloid Interface Sci.*, 2012, **367**, (1), pp. 415–421
[36] Ren Y., Yan N., Feng J., *ET AL.*: 'Adsorption mechanism of copper and lead ions onto graphene nanosheet/δ-MnO_2', *Mater. Chem. Phys.*, 2012, **136**, (2-3), pp. 538–544
[37] Sun W., Li L., Luo C., *ET AL.*: 'Synthesis of magnetic graphene nanocomposites decorated with ionic liquids for fast lead ion removal', *Int. J. Biol. Macromol.*, 2016, **85**, pp. 246–251
[38] Lingamdinne L.P., Koduru J.R., Roh H., *ET AL.*: 'Adsorption removal of Co(II) from waste-water using graphene oxide', *Hydrometallurgy*, 2016, **165**, pp. 90–96
[39] Gao T., Yu J., Zhou Y., *ET AL.*: 'The synthesis of graphene oxide functionalized with dithiocarbamate group and its prominent performance on adsorption of lead ions', *J. Taiwan Inst. Chem. Eng.*, 2017, **71**, pp. 426–432
[40] González M.A., Pavlovic I., Barriga C.: 'Cu(II), Pb(II) and Cd(II) sorption on different layered double hydroxides. a kinetic and thermodynamic study and competing factors', *Chem. Eng. J.*, 2015, **269**, pp. 221–228

doi: 10.1049/mnl.2018.5640